Smart Materials and Structures

PAPER

Achieving high-speed smooth motion for stick-slip piezoelectric motors with impact-enhanced driving mode

To cite this article: Yuzhou Duan *et al* 2025 *Smart Mater. Struct.* **34** 045022

IOP Publishing Smart Materials and Structures
Smart Mater. Struct. **34** (2025) 045022 (11pp) https://doi.org/10.1088/1361-665X/adcd34

Achieving high-speed smooth motion for stick-slip piezoelectric motors with impact-enhanced driving mode

Yuzhou Duan[1], **Jie Ling**[1,*], **Micky Rakotondrabe**[2] **and Yuchuan Zhu**[1,*]

[1] College of Mechanical and Electrical Engineering, Nanjing University of Aeronautics and Astronautics, Nanjing 210016, People's Republic of China
[2] Laboratoire Génie de Production, University of Technology Tarbes Occitanie Pyrénées, University of Toulouse alliance, Tarbes 65016, France

E-mail: meejling@nuaa.edu.cn and meeyczhu@nuaa.cn

Received 30 December 2024, revised 9 April 2025
Accepted for publication 15 April 2025
Published 24 April 2025

Abstract

Stick-slip piezoelectric motors (SSPEMs) are widely regarded as promising candidates for precision positioning systems due to their compact structures and simple driving modes. However, challenges inherent to conventional SSPEMs, including backward motion and instability, seriously limit the output speed of SSPEMs at high driving frequencies. Inspired by the driving principle of impact inertial PEMs, this paper proposes an impact-enhanced driving mode that enables SSPEMs with smoother ripple motion and improved driving frequencies compared to conventional driving modes. The proposed driving mode utilizes the parasitic motion of the compliant mechanism (CM) and the inertia of the driving foot to generate larger force to the mover at high driving frequencies, so that the backward motion can be eliminated and the output performance can be improved at high frequency. To validate the proposed driving mode, an SSPEM with modified triangular configured CM is carefully designed by analytical models and finite element simulation. A prototype is then fabricated for validation. Experimental results show that the backward motion is eliminated when the driving frequency exceeds 800 Hz. Comparative results further highlight the advantages of the impact-enhanced driving mode, achieving a maximum driving frequency of 1800 Hz and a peak velocity of 38.19 mm s^{-1}. The proposed impact-enhanced driving mode offers a universal and effective solution for SSPEMs with parasitic-motion CMs, significantly improving speed, accuracy, and high-frequency one-step stability.

Keywords: piezoelectric motor, high frequency, smooth motion, stick-slip principle

1. Introduction

Piezoelectric actuators (PEAs) have been widely adopted in many precision systems such as microsurgery devices [1], micromanipulators [2], and microinjection devices [3]. Compared with counterparts, PEAs possess merits of high accuracy, compact structure, fast response, and non-electrical radiation [4–6]. Recently, many types of PEAs, ranging from submillimeter-level stroke PEAs (direct drive type [7] and amplified type [8]) to piezoelectric motors (PEMs) with theoretically unlimited stroke, are proposed to keep improving the output performance of accuracy, velocity, and load capacity [9–19].

The basic structure of the PEM consists of a stator and a mover, which interacts through the driving foot. According to the driving modes, current PEMs can be divided into the resonant type with speed advantage and the stepping type with precision advantage. The resonant type is also known as ultrasonic motors, which suffer problems of high frictional wearing loss

* Authors to whom any correspondence should be addressed.

and relatively low positioning resolution. The latter can be further divided into inchworm PEMs [10–12] and inertial PEMs. The inchworm PEMs have multiple piezo-actuated driving feet, which alternately clamp the mover/stator by static friction under a set of control signals. The inertial PEMs commonly adopt compliant mechanisms (CMs) for motion transmission and take advantage of the fast response of piezoelectric ceramics to make the driving foot perform a specified subtle movement in one cycle. In this way, the mover can advance through harmonious coordination of friction and inertia forces.

According to the principle of force coordination, the inertial PEMs can be classified into impact inertial PEMs (IIPEMs) [13–15] and stick-slip PEMs (SSPEMs) [16–19]. The IIPEMs adopt the large inertial force against the friction force to advance, while the SSPEMs leverage the inertia of the mover to realize the conversion of dynamic and static friction. The SSPEM has more compact structures and stable motion than the IIPEM. It utilizes one driving degree of freedom (DOF) and one driving foot to generate a slow-forward-and-fast-backward reciprocating motion. Thus, although the mover moves forward in the slow-forward phase (stick stage), the intrinsic reciprocating motion forces the mover backward in the fast-backward phase (slip stage). This backward motion, on the one hand, reduces the output speed and single-step stability of the SSPEMs, and on the other hand, compromises the motion accuracy per step. Additionally, the step characteristic becomes elusive when the driving frequency goes high, which reduces the motion stability of SSPEMs. Typically, the backward ratio is larger than 40% [20, 21].

As concluded in figure 1, the state-of-the-art methods to suppress or even eliminate the backward motion of SSPEMs can be classified into four categories according to the minimum required number of driving feet and driving DOFs. Achieving backward motion suppression without introducing additional driving DOF/foot is challenging, which involves both control and structural methods. An increase in driving DOFs implies a control-based approach, while an increase in the number of driving feet indicates a structural approach. Increasing both means using multiple independent PEAs to suppress backward motion. The related works are detailedly reviewed as follows:

(1) 1 driving DOF and 1 driving foot. Suppressing backward motion without introducing additional DOF is challenging. For conventional SSPEMs, Xun *et al* indicate that the backward motion can be suppressed by decreasing the dynamic friction, reducing the slip time, or increasing the foot velocity [22]. Zhu *et al* adopt a vibration composite driving signal to reduce the dynamic friction at the slip stage [23]. Cheng *et al* use structural methods, including asymmetric flexure hinge [24] and inertia block structure [25], to reduce the support force between the driving foot and the mover at the slip stage. For unconventional SSPEMs, forward friction is introduced as the competitor to the backward friction at the slip stage due to the system flexibility. Wang *et al* report this phenomenon by changing the preload gap between the stator and the mover and explain this method by establishing an analytical model [26, 27]. Li *et al* successfully suppress the backward motion by the flexure design of the driving foot [28]. Based on the parasitic motion principle, Yang *et al* design an arc-shaped flexure hinge to generate the forward friction [29]. **(2) 1 driving DOF and 2 driving feet**. Based on the Stribeck effect, Tian *et al* use a passive foot to clamp the mover at the slip stage. Although they use two driving DOFs, one is enough to implement this principle [30]. **(3) 2 driving DOFs and 1 driving foot**. When one extra DOF is introduced in driving the driving feet, the monotonous reciprocating trajectory of the driving foot can be replaced by a closed curve trajectory, such as the rectangular [31] and elliptical trajectories [32]. Therefore, the return error can be eliminated in principle. **(4) 2 driving DOFs and 2 driving feet**. Two active driving feet mean they can work in tandem to conduct complex locomotion to suppress the backward motion. One current solution uses two same conventional SSPEMs but applies phase-shifted driving signals [33–36]. Inspired by the walking motion of the human legs, Li *et al* utilize two L-shaped flexure mechanisms with different phases to suppress backward motion [37]. In [38], the design principle of using two driving feet to generate elliptical motion in an alternating pattern is proposed to achieve continuous linear motion of the actuator. Another solution utilizes an inchworm/stick-slip compound method, which adopts an extra active clamping mechanism to clamp the mover at the slip stage [39, 40].

Certain of the aforementioned studies have successfully suppressed and even eliminated the backward motion. However, these methods either increase driving/structural DOFs [30–36, 39, 40], tend to cause unstable burst motion (although the burst motion can increase step size) [26–29], or are not competitive on speed ($\leqslant$ 8.6 mm s^{-1}) [22–25]. The increased DOF will inevitably lead to complex mechanical structures. The inherent stick-slip driving pattern and the burst motion both bring motion instability in one single step. Hence, simultaneously achieving high-speed stick-slip motion and eliminating the backward motion, while maintaining the simple structure and motion smoothness of SSPEMs remains unsolved.

Inspired by the driving principle of IIPEMs, this paper proposes an impact-enhanced driving mode to suppress the backward motion of SSPEM without increasing the driving DOFs and feet, and enables high-speed smooth motion. Both an inertial driving foot and a CM with parasitic motion contribute to conducting the impact-enhanced motion. The triangular-configured CM (TCCM) is proposed by [16] and has been used in our previous work [1], which can generate parasitic motion with simple structure. Therefore a modified TCCM is designed, modeled, and simulated to validate the proposed driving mode in this paper. In comparison with existing works in [29, 30, 39–41], the developed motor has competitive output performance in smooth motion with better velocity, output force, and locking force. The main contributions of this paper can be organized as follows:

- Proposing an impact-enhanced driving mode suitable for SSPEMs with a parasitic motion CM and an inertial driving foot. By adopting this driving mode, SSPEMs can achieve a higher operating frequency than traditional driving mode, as well as smoother and faster motion.

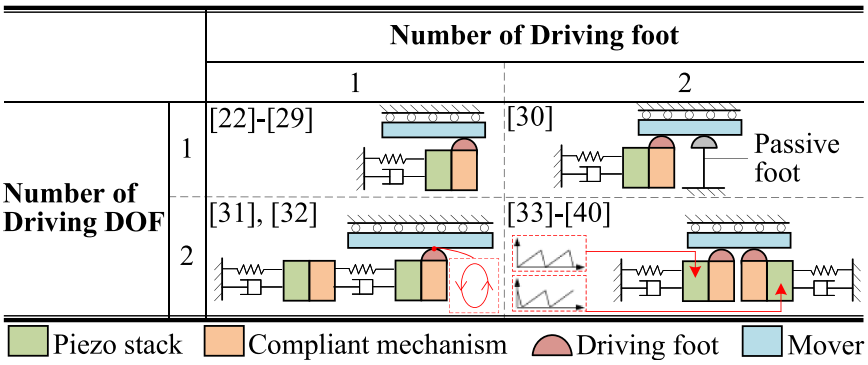

Figure 1. Classification of the advanced methods for backward motion suppression according to the number of driving feet and DOFs.

- Developing an SSPEM with a modified TCCM that can implement impact-enhanced driving mode. Analytical models including the stiffness model and dynamic model are established for design requirements and validated by simulations and experiments.
- Achieving backward motion elimination, velocity increase, and motion smoothness simultaneously at high frequencies based on the proposed SSPEM driven by the impact-enhanced driving mode.

The remainder is organized as follows. Section 2 introduces the system configuration and working principle. In section 3, the analytical models of the TCCM, including stiffness and dynamics, are established. The stiffness model is established to determine an appropriate stiffness relationship between different flexure hinges and piezo stacks for driving the proposed SSPEM, while the dynamic model provides the system's first-order natural frequency to accommodate various design requirements. Then, finite element simulations are conducted in section 4 to validate the analytical models of the modified TCCM, and the feasibility of the proposed impact-enhanced driving mode. In section 5, a prototype is fabricated and its output performance based on the impact-enhanced driving mode is tested under different driving voltages, driving frequencies, and loads in comparison with the conventional driving mode. Last, section 6 compares our work with other advanced methods for suppressing backward motion. and concludes the article.

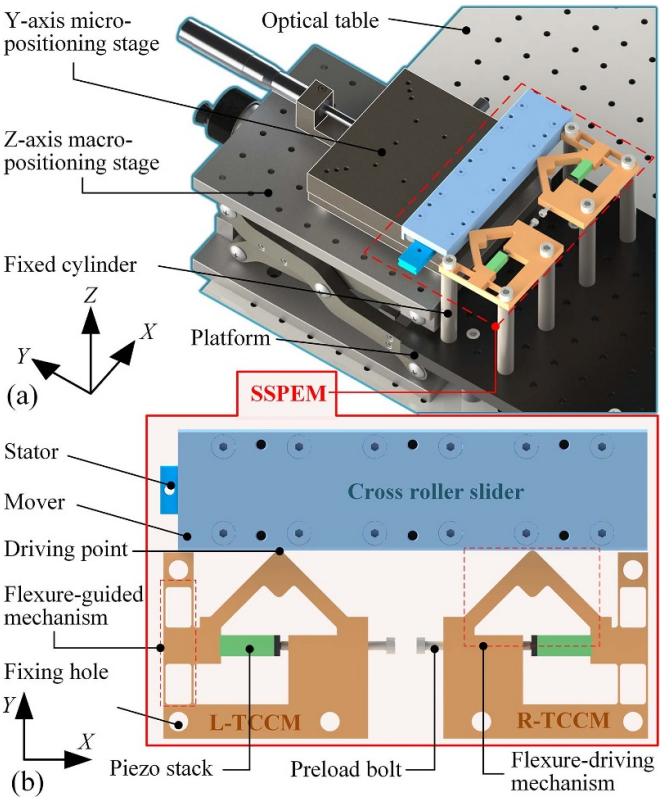

Figure 2. Computer-aided design model of the proposed system. (a) System configuration. (b) Detailed structure of the proposed stick-slip piezoelectric motor (SSPEM). Abbreviation: L, left; R, right; TCCM, triangular-configured compliant mechanism.

2. System structure and working principle

2.1. System structure

Figure 2 presents presents the computer-aided design model of the proposed SSPEM system. As shown in figure 2(a), the system is fixed on the optical table. Six fixed columns are introduced to fix the two TCCMs and to avoid the possible friction between the SSPEM and the platform. Furthermore, the fixed cylinders are installed on a platform for vibration isolation. A Z-axis macro-positioning stage and a Y-axis micro-positioning stage are introduced to adjust the slider position. The details of the SSPEM are depicted in figure 2(b), where two identical TCCMs, i.e. left-TCCM and right-TCCM (L-TCCM and R-TCCM) are mounted symmetrically. For each TCCM, a piezo stack is preloaded by the preload bolt and provides motion input to the TCCM. The input is constrained laterally by a flexure-guided mechanism and transforms to the coupled motion in the X- and Y-directions with the help of a flexure-driving mechanism. The parasitic motion in the Y-direction helps to generate the impact-enhanced motion.

Of note, one TCCM is enough to implement the impact-enhanced motion. The extra TCCM is introduced in the system for comparison tests in section 5 as well as test the consistency of the bidirectional motion. To avoid the interference of the

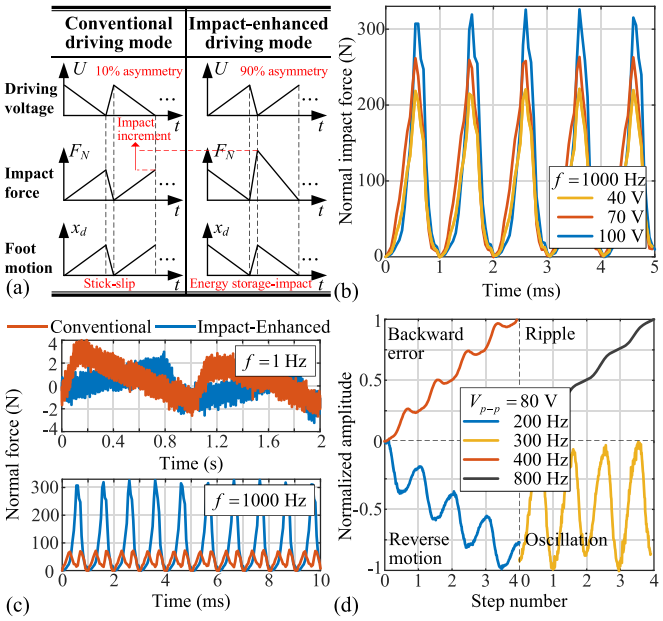

Figure 3. Experimental results demonstrate the principle of the impact-enhanced driving mode. (a) Comparison of the proposed mode and conventional one. (b) Normal impact force under different driving voltage. (c) Comparison of normal impact force of two driving modes at different frequencies. (d) Evolution of the step characteristics as the driving frequency increases.

non-working TCCM on the slider, its driving point is detached from the slider by applying a large voltage.

2.2. Principle of the impact-enhanced driving mode

Figure 3 introduces the principle of the impact-enhanced driving mode. As presented in figures 3(a), under the driving signal of the 10% asymmetric triangular wave, the proposed motor conducts conventional stick-slip motion. Under the driving signal of the 90% asymmetric triangular wave, the driving foot performs impact-enhanced motion with the help of the specially designed TCCM. The TCCM can produce parasitic motion in the Y-direction and has a driving foot with a certain mass. Driven by the piezo stack, the TCCM stores energy and then impacts the slider. Due to the inertial effect of the driving foot, the impact-enhanced motion generates additional impact force increment to move the slider forward in comparison with the conventional one. Therefore, the driving force under the impact-enhanced driving mode is much larger than the conventional mode. Although it is difficult to explicitly model the incremental impact force, intuitively, the impact force is positively correlated with both the driving frequency and the voltage (considering the inertial effect). To prove it, the normal contact force of the two driving modes is measured experimentally under different driving voltages/frequencies. The results are presented in figures 3(b) and (c), which prove the existence of incremental impact force. Additionally, the normal impact force increases significantly with the increase in driving frequency and voltage (from 4 N to 300 N).

When the impact increment is not significant, the motor would output conventional stick-slip motion in the opposite direction, even in the impact-enhanced drive mode. As aforementioned, the impact effect remarkably increases with the driving frequency. Therefore, as the frequency increases, the competitive relationship between the impact-enhanced motion and the conventional motion leads to the evolution of step characteristics. As shown in figure 3(d), four different step characteristics would appear successively as the driving frequency increases. At 200 Hz, the leading motion is the conventional one and gradually turns to impact-enhanced motion at 400 Hz. With the enhancement of the impact force, the backward error begins to disappear and the motion becomes smooth when the driving frequency exceeds 800 Hz.

2.3. Working principle

Driven by triangular waves with different asymmetry, the designed SSPEM could either perform the conventional stick-slip motion or the impact-enhanced stick-slip motion. As illustrated in figure 4, the working principles based on the two modes are summarized as follows, which mainly include three steps. To better reflect the slider motion, its displacement is amplified.

Initial stage: the initial state of any stable working cycle. For conventional mode, the piezo stack has been actuated. The slider is separated from the driving foot and has a certain backward speed. For the impact-enhanced mode, the piezo stack is not actuated. There is an initial preload between the driving foot and the slider. The slider has a certain forward speed.

Step C1/I1: the former phase of any stable working cycle. For conventional mode, the voltage applied to the piezo stack slowly decreases, which causes the TCCM to return to the initial state. Thus, the driving foot would contact with the slider and generate forward friction to stick the slider forward. For the impact-enhanced mode, as the voltage slowly increases, the drive foot would separate from the slider. Although departing the driving foot would cause backward friction on the slider, this effect is submerged in the initial velocity. The elastic potential energy of the TCCM gradually increases.

Step C2/I2: the latter phase of any stable working cycle. For conventional mode, as the voltage on the piezo stack rapidly increases. The drive foot quickly separates from the slider, which causes backward motion. For the impact-enhanced mode, the voltage suddenly decreases. The energy stored in TCCM is released to generate a rapid impact between the slider and the driving foot. As proofed in section 2.2, this impact-enhanced motion would generate a large forward impact force to move the slider forward.

As elaborately presented in figure 4(d), the impact-enhanced driving mode provides a two-phase-forward smooth motion ($d_i = d_{i1} + d_{i2}$) instead of the forward-backward motion ($d_c = d_{c1} - d_{c2}$) of the conventional mode.

3. Modeling and design

In this section, first, the analytical model of the TCCM is proposed for design requirements, including the stiffness

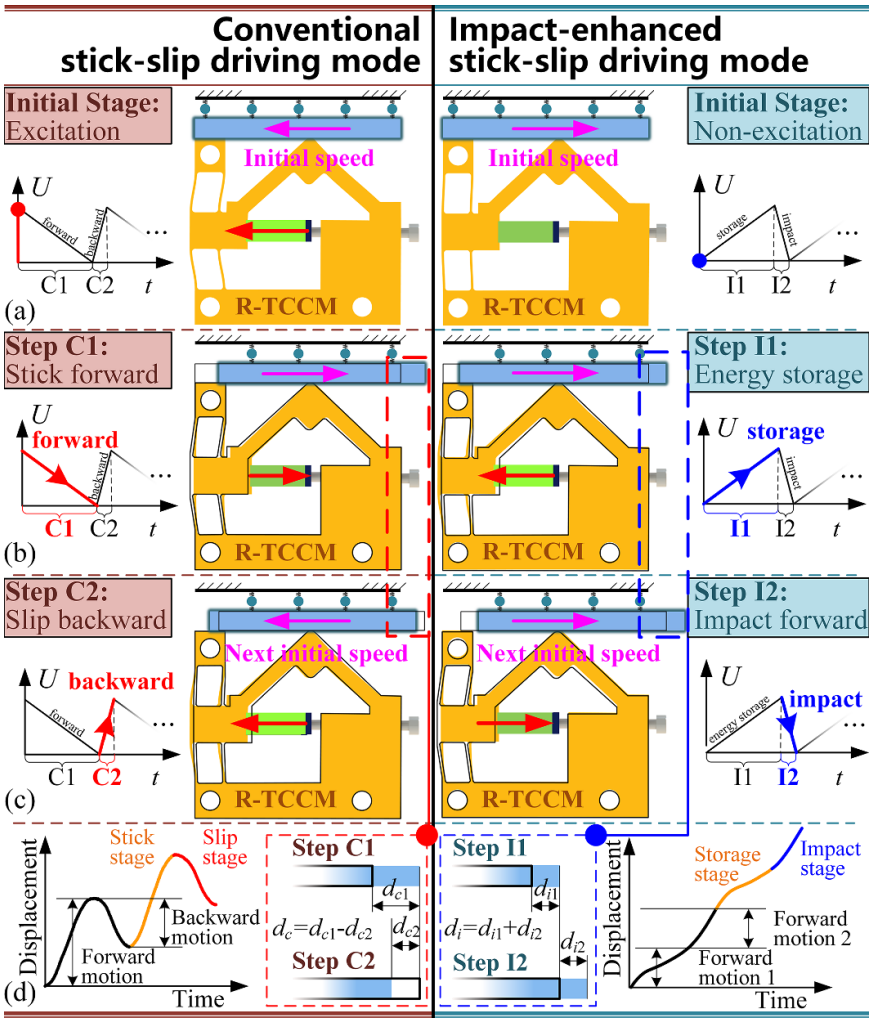

Figure 4. Comparison of working principle of the two driving modes. (a) Initial stage. (b) Step C1/I1: stick forward/energy storage. (c) Step C2/I2: slip backward/impact forward. (d) Different step characteristics of the two modes.

and dynamics (natural frequency). The stiffness model contributes to realizing the impact-enhanced driving mode as well as ensuring that the stiffness of TCCM matches the piezo stack and the X-direction movement of the piezo stack. The dynamic model derives the first order natural frequency of the TCCM, which determines the maximum working frequency of the SSPEM. Last, the TCCM with designed parameters is validated first by finite element simulations.

3.1. Analytical modeling of the TCCM

As presented in figures 5(a) and (b), the analytical models of the TCCM, including statics and dynamics, are established for design purposes in section 3.2. It is assumed that the flexure-guided mechanism plays an ideal guiding role, and the flexure-driving mechanism is regarded as the ideal Timoshenko beam. Then, the relationship of the input and output of the TCCM can be expressed as

$$x_2 = \frac{x_1}{2}, y_2 = x_2 \tan\frac{\theta}{2} \tag{1}$$

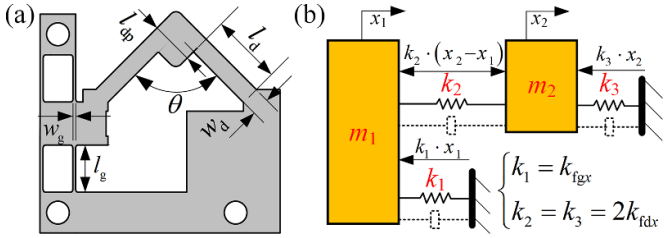

Figure 5. Analytical model of the triangular-configured compliant mechanism (TCCM). (a) Geometric parameters of the TCCM. (b) Dynamic model of the TCCM.

where x_1 and x_2 are the input and output displacements in the X-direction, respectively. y_2 is the output displacements in the Y-direction. θ is the driving angle of the TCCM. It can be seen from (1) that increasing the required parasitic motion and forward impact force are in conflict. Consequently, the driving angle θ is selected to be 90°.

3.1.1. Stiffness modeling. All flexible beams are assumed to be Euler-Bernoulli beams because they are fixed at both ends

Table 1. Analytical, simulation, and experimental values of the designed parameters of the compliant mechanism.

Design parameters	Analytical value	Simulation value	Experimental value
k_{fgx}	0.80 N μm^{-1}	0.87 N μm^{-1}	0.84 N μm^{-1}
k_{fgy}	80.0 N μm^{-1}	71.4 N μm^{-1}	73.1 N μm^{-1}
k_{fdx}	12.0 N μm^{-1}	10.8 N μm^{-1}	11.2 N μm^{-1}
f	2.70 kHz	3.10 kHz	2.96 kHz
α	10.0	11.1	10.7
β	15.0	12.4	13.3
γ	100	89.3	82.1
θ	90.0°	88.3°	91.2°

of the mass block (assumed rigid). The analytical expressions for the stiffness of the TCCM are presented as follows:

$$k_{fgx}=\frac{4Ew_g^3t}{l_g^3},k_{fgy}=\frac{4Ew_gt^3}{l_g^3},k_{fdx}=\frac{1}{4}k_{fdy}=\frac{Ew_d^3t}{2l_d^3} \tag{2}$$

where k_{fgx}, k_{fgy}, k_{fdx}, and k_{fdy} are the stiffness of the flexure-guided mechanism and the flexure-driving mechanism in X-direction and Y-direction, respectively. w_g and l_g are the width and length of the flexure-guided mechanism. w_d and l_d are the width and length of the flexure-driving mechanism. t is the thickness of the TCCM. E is the Young's modulus.

3.1.2. Dynamic modeling. Figure 5(b) shows the simplified physical model of the proposed TCCM. The Lagrange's equations of the system can be expressed as

$$\begin{cases}\dfrac{\mathrm{d}}{\mathrm{d}t}\left(\dfrac{\partial(T-V)}{\partial\dot{x}_1}\right)-\dfrac{\partial(T-V)}{\partial x_1}=0\\ \dfrac{\mathrm{d}}{\mathrm{d}t}\left(\dfrac{\partial(T-V)}{\partial\dot{x}_2}\right)-\dfrac{\partial(T-V)}{\partial x_2}=0\end{cases} \tag{3}$$

where

$$T=m_1\dot{x_1}^2+m_2\dot{x_2}^2,V=\frac{1}{2}k_1x_1^2+\frac{1}{2}k_2\left(x_2-x_1\right)^2+\frac{1}{2}k_3x_2^2. \tag{4}$$

where m_1 and m_2 are the system masses calculated by the lumped parameter method. k_1, k_2, and k_3 are the system stiffness, which have $k_1=k_{fgx},k_2=k_3=2k_{fdx}$. Sorting out (3), the following equation about $X=[x_1,x_2]'$ can be derived:

$$M\ddot{X}+KX=0 \tag{5}$$

with

$$M=\begin{bmatrix}m_1&0\\0&m_2\end{bmatrix},K=\begin{bmatrix}k_1+k_2&-k_2\\-k_2&k_2+k_3\end{bmatrix}. \tag{6}$$

According to section 3.2 that $k_1\ll k_2$, the simplified form of the natural frequency ω can be derived by letting $\det\left(K-\omega^2M\right)=0$:

$$w=\sqrt{\frac{2k_2m_1+k_2m_2-\sqrt{\left(2k_2m_1+k_2m_2\right)^2-4{k_2}^2m_1m_2}}{2m_1m_2}}. \tag{7}$$

3.2. Design

First, the X-direction stiffness of the TCCM needs to be designed. On the one hand, the flexure-driving mechanism provides enough preload for the piezo stack, and on the other hand, it generates enough driving force for the slider. Additionally, the flexible-guided mechanism should be regarded as an ideal moving pair, that is, its stiffness in the X-direction should be ignored. Then we have k_p =120 N μm^{-1} $\gg k_{fdx}\gg k_{fgx}$ (k_p is the stiffness of the piezo stack used in this paper).

Second, the flexible-guided mechanism should be regarded as an ideal moving pair. Thus one have $k_{fgy}\gg k_{fdx}\gg k_{fgx}$. For brevity, we use three stiffness ratios (α,β,γ) to describe the aforementioned relationship, which takes the form

$$\alpha=\frac{k_p}{k_{fdx}},\beta=\frac{k_{fdx}}{k_{fgx}},\gamma=\frac{k_{fgy}}{k_{fgx}}. \tag{8}$$

Last, the natural frequency of the TCCM requires to be designed relatively high to enable high-frequency actuation. Here, we adjust this value based on the trial-and-error method. We set the value of the first order natural frequency as 3.1 kHz. Therefore, the maximum operating frequency of the proposed SSPEM is half of the design natural frequency. This is because the driving signal of asymmetric triangular wave contains a lot of higher-order harmonic components, and the second-order harmonic component would seriously affect the output performance. Following the above design principles, we put forward the design indexes (analytical value) in table 1.

4. Finite element simulation

In section 3, the specific parameters of the TCCM are selected. In this section, finite element simulations are carried out in the COMSOL environment to validate the design process and validated the proposed driving mode. First, static and dynamic simulations are conducted to validate the analytical models of the modified TCCM. Then, the computer-aided design platform in figure 2 is simplified and simulated in dynamic conditions to validate the proposed impact-enhanced driving mode in comparison with the conditional driving mode.

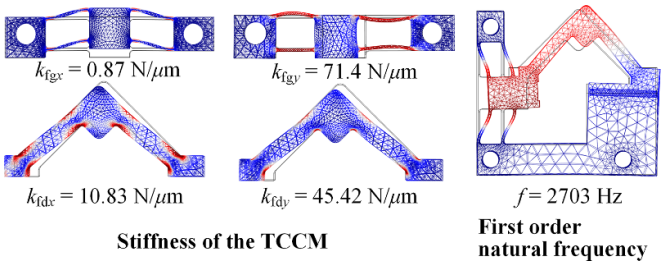

Figure 6. Simulation of the stiffness and natural frequency of the modified triangular configured compliant mechanism (TCCM).

Table 2. Geometric parameters of the designed system.

Parameter	Value	Parameter	Value	Parameter	Value
w_g	0.7 mm	l_d	20 mm	θ	90°
w_d	5.0 mm	l_g	13.2 mm	m_1	27.8 g
t	7.0 mm	l_{dp}	12 mm	m_2	21.7 g

4.1. TCCM simulation

In this part, the previously established static and dynamic model of the modified TCCM is validated through simulation. As shown in figure 6, a single TCCM is introduced in COMSOL to test the stiffness of the flexure-guided mechanism, the flexure-driving mechanism, and the first order natural frequency. Table 2 presented the simulated results, which are compared with the previously derived analytical results, as well as the experimental results derived from section 5. The average error of the three methods is 11%. The material parameter errors, boundary condition deviations, and manufacturing-induced errors mainly cause the deviations.

4.2. System simulation

In this part, the whole SSPEM is simulated in a dynamic environment under both conventional and impact-enhanced driving modes. The input signal is 90% asymmetric triangular wave under different driving frequencies. The models are manually meshed with the contacts and flexure hinges refined as shown in figure 7(a). The TCCM is fixed through its bolt holes, and the slider is simplified as an equivalent rigid body with the same mass. A preload displacement of 3.75 μm is applied in the contact direction to ensure consistency with the experiment. The friction relationship between the TCCM and the slider is defined, with the friction coefficient set to 0.21 based on a trial-and-error method.

Then, the two driving modes are tested in the simulation environment. Figure 7(b) presents the simulation results of the displacement cloud map in the slider's motion direction under conventional stick-slip mode. Here, we assume the piezo stack to be perfectly ideal, producing a displacement of 14.9 μm at 80 V. The driving frequency is set to 100 Hz. The results show that the slider moves forward by 11.8 μm during the stick stage and moves backward by 6.1 μm during the slip stage. To validate the fact that the impact effect remarkably increases with the driving frequency, the normal force between the driving foot

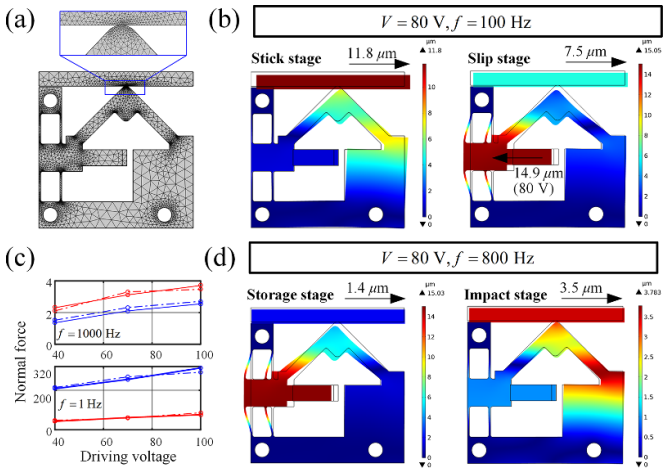

Figure 7. Dynamic simulation of the impact-enhanced driving mode of the proposed stick-slip piezoelectric motor (SSPEM). (a) The meshed SSPEM. (b) Dynamic simulation of the proposed SSPEM under conventional driving mode. (c) Comparison of the normal force under two driving mode through simulation and experiment. The red lines represent the conventional results and the blue lines represent the proposed method. The solid lines represent the experimental results, and the dotted lines represent the simulation results. (d) Dynamic simulation of the proposed SSPEM under impact-enhanced driving mode.

and the slider under impact-enhanced driving mode is simulated and experimentally tested. The tests are conducted under driving voltages of 40, 70, and 100 V and driving frequencies of 1 Hz and 1000 Hz. Figure 7(c) presents the results, which confirm that the impact-driven principle can indeed enhance the normal force between the driving foot and the slider at high frequencies, thereby increasing the maximum operating frequency and speed of the SSPEM. The average error between simulation and experiments is 7.7%. Figure 7(d) shows the displacement cloud map under impact-enhanced stick-slip mode under the driving frequency of 800 Hz. The results show that at the storage stage, the slider moves forward by 1.4 μm due to its initial speed, and at the impact stage, the slider moves forward by 6.1 μm.

5. Experimental test

5.1. Setups

Figure 8 presents the experiment systems. As shown in figures 8(a) and (b), A PC-DAQ system (PCI-6259, NI, USA) is used to generate the driving signals of the two piezo stacks (SA070718, PiezoDrive, Australia), which are amplified by two power amplifiers (7224, AE Techron, USA). The macro displacement signal is measured by a laser sensor (CD33-120NV, OPTEX, Japan), and the micro displacement signal is measured by a capacitive sensor (10^{-09}.CAP200, Core Tomorrow, China). Figure 8(c) presents the enlarged view of the prototype. The TCCM is made of 65Mn and fabricated via wire-cut electrical discharge machining. A flexible piezoresistive force sensor (A201, Tekscan, USA) is used to measure the contact force between the driving feet and the slider

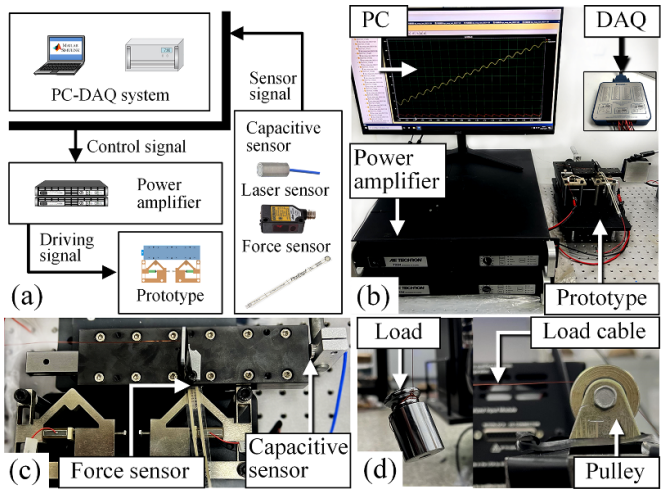

Figure 8. The configuration of the experimental system. (a) The signal flow diagram. (b) Established experimental system. (c) Enlarged view of the prototype. (d) The load test preparation.

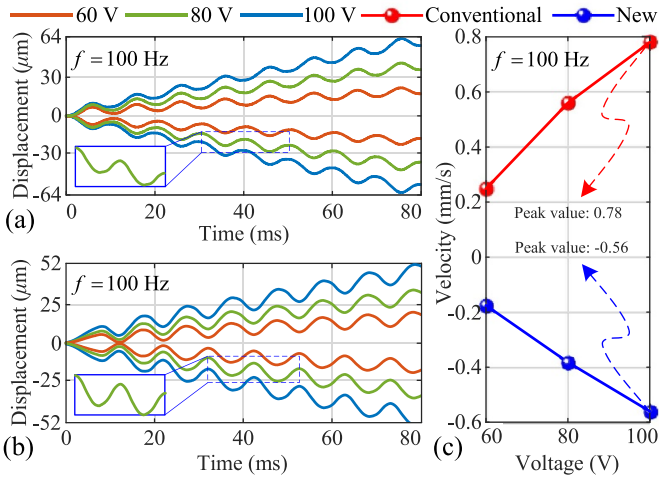

Figure 9. Experimental results of the effect of the driving voltage on slider motion at low frequency (100 Hz) and bidirectional motion consistency tests. (a) Bidirectional micro displacement under conventional driving mode. (b) Bidirectional micro displacement under impact enhancement driving mode. (c) Velocity under two driving modes.

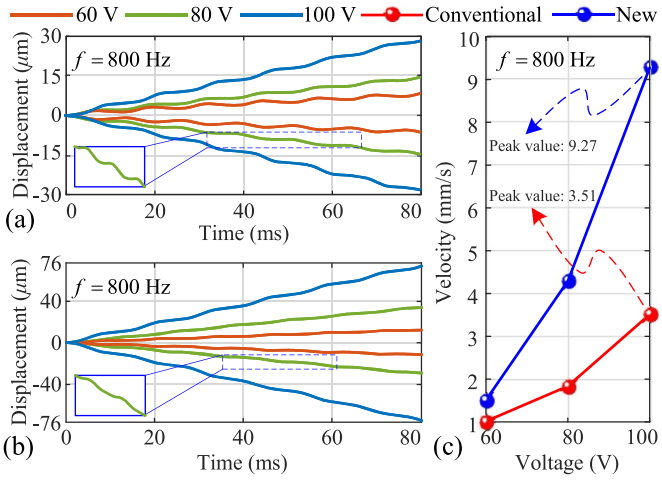

Figure 10. Experimental results of the effect of the driving voltage on slider motion at high frequency (800 Hz) and bidirectional motion consistency tests. (a) Bidirectional micro displacement under conventional driving mode. (b) Bidirectional micro displacement under impact enhancement driving mode. (c) Velocity under two driving modes.

(CHTA, SAMLO, China) to guarantee assembly consistency. Figure 8(d) shows the load, pulley, and cable used in the load test. An asymmetric triangular wave is adopted in the following experiments. Notably, excessive asymmetry may lead to damage in the piezoelectric stacks, while insufficient asymmetry would weaken the driving capability. Therefore, the asymmetry of 10% is chosen in the following tests.

The preload of the system is an important factor affecting the accuracy and performance of the system. For the preload of the piezo stack, we set the preload to 30% of its blocking force (540 N) and achieved this by measuring the displacement of the flexure-guided mechanism using a capacitive sensor and utilizing the CM stiffness obtained earlier. The preload between the driving foot and the slider is adjusted by the *Y*-axis micro-positioning stage. We set the operating voltage of the piezo stack to 60–100 V to ensure a relatively large displacement output and guarantee safety. To ensure that our proposed model can be implemented, 40 V voltage (below the lower working frequency) is applied in the preparation stage to both piezo stacks. Then, we make the driving feet contact with the slider by operating the *Y*-axis stage. Finally, we reduce the driving voltage to zero. In the following tests, the working voltage is between 60 and 100 V to achieve the impact-enhanced motion. Additionally, when one driving foot is operated, a 120 V voltage is applied to the piezo stack of another driving foot to eliminate its interaction.

5.2. *Performance test of conventional and new driving mode*

5.2.1. Effect of voltage. Figures 9 and 10 present the effect of the driving voltage on slider motion at low frequency (100 Hz) and high frequency (800 Hz). The bidirectional motion consistency of the two driving feet is also tested. As shown in figure 9, the two driving modes exhibit similar stick-slip characteristics at low frequencies and have relatively large backward motion. As the driving voltage increases, the slider speed increases in an approximately linear manner. In comparison with conventional driving mode, the proposed driving mode has a larger backward error. This may be due to the gradual reduction of the normal force of the driving foot on the slider during the stick stage.

As shown in figure 10, both the backward motion of the two driving modes disappears. At this time, the microscopic output displacement is ripple-shaped. For the conventional method, this ripple phenomenon has been reported in [22]. According to figure 11, when the driving frequency is larger than 800 Hz, the backward motion begins to increase rapidly and the slider stops moving. For the impact-enhanced method, 800 Hz is

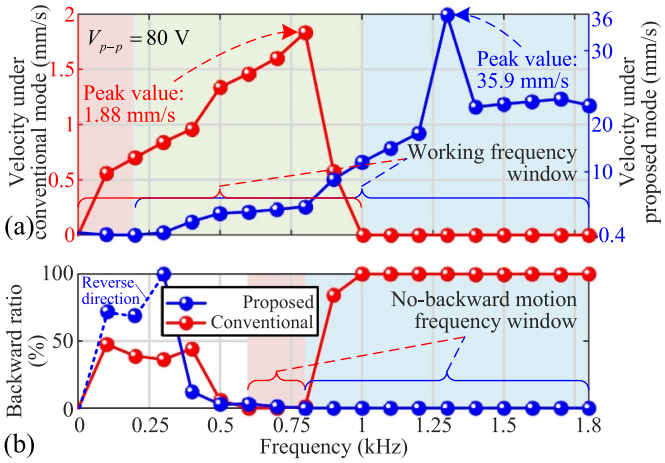

Figure 11. Experimental results of the effect of the driving frequency on the speed and backward ratio of the slider under the proposed driving mode at the voltage of 80 V. (a) Effect on slider speed. (b) Effect on the backward ratio of the slider.

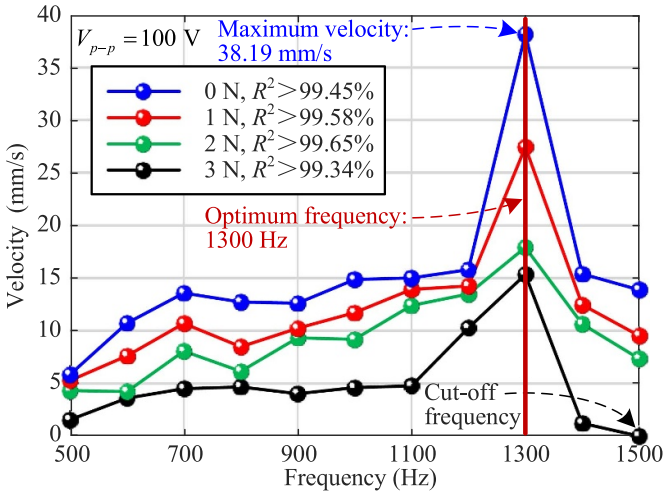

Figure 12. Experimental results of the effect of the load on slider speed at different frequencies from 500 Hz to 1500 Hz.

the start frequency for the high-speed smooth motion. From figures 9 and 10 it can be concluded that the bidirectional consistency of the two SSPEMs is good, which is closely related to the manufacturing process (the two TCCMs are wire-cut together), and the installation depicted in experimental setups.

5.2.2. Effect of frequency. The slider speeds and backward ratios (the ratio of backward displacement to maximum forward displacement in one step, also noticed as step efficiency) under different driving frequencies ranging from 100 Hz to 1800 Hz are tested with a driving voltage of 80 V, and the results are summarized in figure 11. This figure shows that the starting frequency of the proposed driving mode is 300 Hz. From 300 Hz to 800 Hz, the backward ratio quickly drops to very small ($\leqslant$3.2%) and decreases to zero. This phenomenon is normal in SSPEMs, for the backward motion could be suppressed or even eliminated by increasing the velocity in the stick state [22]. Although the frequency test stops due to piezoelectric heating, the proposed method already operates at twice the frequency of the conventional method (1800 Hz versus 900 Hz). The no-backward-motion frequency window of the impact-enhanced method is four times larger than the conventional method (1000 Hz versus 200 Hz). Additionally, the maximum velocity under the proposed driving mode is approximately 20 times that of the conventional one (35.9 mm s^{-1} at 1300 Hz versus 1.88 mm s^{-1} at 800 Hz).

5.2.3. Effect of load. Load tests are carried out to measure the output force and locking force of the proposed SSPEM under the impact-enhanced driving mode. The maximum output force is 4.1 N with a very slow speed (0.2 mm s^{-1}). The maximum locking force (19.1 N) is much larger than the output force due to the self-locking characteristics of the proposed motor. The load tests are conducted with a driving voltage of 100 V and a driving frequency of 500 Hz to 1500 Hz (the cut-off frequency when the load is 3 N). The results in figure 12 show that as the load increases, the speed of the slider decreases gradually. The optimum frequency for high-speed motion is 1300 Hz, and the maximum velocity of 38.19 mm s^{-1} appears when the load is 0 N. This is because the driving signal of asymmetric triangular wave contains a lot of higher-order harmonic components, and at 1300 Hz the second-order component (2600 Hz) reaches the bandwidth of the TCCM. Of each independent point in figure 12, the values of *R*-squared show that the proposed SSPEM has a good linearity in velocity even when the load is relatively large.

6. Discussion and conclusion

6.1. Discussion

Table 3 lists the comparison between this work and other advanced works in suppressing backward motion since 2020. Important motor parameters including speed, locking force, output force, driving DOFs, and size are investigated. For each work, the backward motion is suppressed by one of the methods summarized in figure 1. Most of the current studies validate their motors' performance of suppressing backward motion under low frequency (e.g. 5 Hz). In our work, the backward ratio is zero from 300 Hz to 1800 Hz. Additionally, the developed SSPEM with impact-enhanced driving mode possesses extremely competitive speed (38.19 mm s^{-1}) and locking force (19.1 N). The large locking force is due to the self-locking characteristics of the proposed TCCM, which is in wide demand in many fields, including safety requirements in surgical robotics. Meanwhile, the proposed motor can provide considerable output force. The above excellent properties can be achieved by using one piezo stack and one CM.

Although the impact-enhanced driving mode proposed in this paper demonstrated greater advantages over the conventional driving mode in experiments, including higher operating frequency, improved one-step stability, and faster speed, its

Table 3. Comparison between this work and other state-of-the-art works contributed to suppress the backward motion since 2020

Reference	This work	[30]	[29]	[40]	[39]	[41]
Year	N/A	2022	2020	2023	2021	2022
Method	Impact-enhanced	Passive foot	Parasitic motion	Epicycloid induction	Active locking	Flexible beam
Backward ratio	0% ($\geqslant$300 Hz)	$\leqslant$1% (5 Hz)	0% (5 Hz)	$\leqslant$1% (1 Hz)	3.66% (mostly)	0 (10 Hz)
Speed (mm s^{-1})	38.19 (1300 Hz)	4.18 (200 Hz)	0.175 (25 Hz)	0.15 (5 Hz)	2.26 (700 Hz)	23.7 (400 Hz)
Locking force (N)	19.1	5.4	N/A	N/A	N/A	1.2
Output force (N)	4.1	N/A	1.6	N/A	1.6	3.9
Driving DOFs	1	1	1	2	2	2
Resolution (nm)		4.16	N/A	160	N/A	N/A
Size (mm^3)	$67 \times 102 \times 15$	$118 \times 75 \times 41.5$	$60 \times 35 \times 5$	$90 \times 70 \times 7$	N/A	$90 \times 90 \times 12$

applicability to SSPEMs is limited. Specifically, the SSPEM must be driven by a CM, and this compliant mechanism must exhibit parasitic motion. Additionally, the method is more effective when the driving foot has a considerable mass. Notably, CMs that generate parasitic motion are typically asymmetric, which often results in inconsistent motion capabilities in two directions. This asymmetry may impose limitations on certain applications, such as those requiring high-speed bidirectional motion.

Moreover, although our proposed method expands the no-backward-motion frequency window, this is achieved by increasing the maximum operating frequency. At low frequencies, backward error still persists when using the proposed method. Therefore, the contribution of this study lies in enabling high-speed smooth motion of SSPEMs, which also constitutes a limitation of this work.

Finally, this study also faces the common issue of significant noise and vibration in SSPEMs during high-frequency operation, which may be exacerbated by the impact-enhanced driving mode. Since our prototype is at a laboratory scale, the innovation of this work lies in proposing a novel driving mode rather than conducting long-term stability tests, which will be one of the focuses of future work.

6.2. Conclusion

This paper proposed an impact-enhanced driving mode, together with a TCCM with parasitic motion, that can eliminate the intrinsic backward motion of conventional SSPEM and achieve high-speed smooth motion. Driven by a 90% asymmetric triangular wave, the TCCM periodically stores energy and impacts the slider through a driving foot with a certain mass. A prototype is designed and fabricated to validate the impact-enhanced driving mode and to test the performance of the proposed motor. Experimental results validate the effectiveness of suppressing backward motion and achieving high-speed smooth motion. The established prototype shows a maximum speed of 38.19 mm s^{-1} at 1300 Hz, a maximum output force of 4.1 N, and a maximum locking force of 19.1 N. Compared with other state-of-the-art methods, this impact-enhanced method is simpler in mechanical structure and driving DOFs, and has competitive output performance in velocity, one-step stability, output force, and locking force.

For future work, on the one hand, we will conduct physical modeling of the proposed impact-enhanced driving mode. On the other hand, based on the platform developed in this paper, we will explore the collaboration of the two driving feet, including the output performance under different driving feet locomotion.

Data availability statement

The data cannot be made publicly available upon publication because they are not available in a format that is sufficiently accessible or reusable by other researchers. The data that support the findings of this study are available upon reasonable request from the authors.

Acknowledgments

This work was supported by the Natural Science Foundation of Jiangsu Province (Grant No. BK20210294), the International Joint Laboratory of Sustainable Manufacturing, Ministry of Education and the Fundamental Research Funds for the Central Universities (Grant No. NG2024016), the Aeronautical Science Foundation of China (Grant No. 20220007052001), and the Postgraduate Research & Practice Innovation Program of Jiangsu Province. (Grant No. KYCX24_0556).

ORCID iDs

Yuzhou Duan https://orcid.org/0009-0003-6056-9119
Jie Ling https://orcid.org/0000-0002-6786-0422
Micky Rakotondrabe https://orcid.org/0000-0002-6413-7271
Yuchuan Zhu https://orcid.org/0000-0002-7399-1656

References

[1] Duan Y, Ling J and Zhu Y 2024 *J. Med. Devices* **18** 034501
[2] Ye T, Feng Z, Ling J and Li Y 2024 *IEEE/ASME Trans. Mechatronics* (Early Access) (https://doi.org/10.1109/TMECH.2024.3476332)
[3] Duan Y, Zhang Y, Ling J, Feng Z and Zhu Y 2022 A hub-type compliant piezo drill for cell microinjection *2022 Int. Conf. on Advanced Robotics and Mechatronics (ICARM)* (IEEE) pp 319–24

[4] Ling J, Feng Z, Chen L, Zhu Y and Pan Y 2023 *Precis. Eng.* **81** 112–23
[5] Zhang Y, Ling J, Feng Z and Zhu Y 2023 A comparison of hysteresis models with the hammerstein structure for piezoelectric actuators *Int. Conf. on Advanced Robotics and Mechatronics (ICARM)* pp 675–80
[6] Li Y, Ye T, Ling J, Xiao X and Feng Z 2024 *Precis. Eng.* **88** 674–85
[7] Zhang Y, Ling J and Zhu Y 2024 *Smart Mater. Struct.* **33** 095003
[8] Ling M, He X, Wu M and Cao L 2022 *IEEE/ASME Trans. Mechatronics* **27** 4942–50
[9] Rakotondrabe M, Haddab Y and Lutz P 2009 *IEEE/ASME Trans. Mechatronics* **14** 733–45
[10] Ling J, Chen L, Feng Z and Zhu Y 2022 *Mech. Mach. Theory* **176** 104997
[11] Dong H, Li T, Wang Z and Ning Y 2020 *Sens. Actuators* A **306** 111950
[12] Ma X, Liu Y, Deng J, Zhang S and Liu J 2022 *Mech. Syst. Signal Process.* **169** 108636
[13] Li J, Zhang S, Liu Y, Deng J and Ma X 2022 *Smart Mater. Struct.* **31** 095008
[14] Shao Y, Shao S, Xu M, Song S and Tian Z 2019 *Smart Mater. Struct.* **28** 055023
[15] Huang X, Hu Y, Ma J, Li J, Lin H and Wen J 2021 *Smart Mater. Struct.* **30** 095014
[16] Zhang Y, Peng Y, Sun Z and Yu H 2019 *IEEE Trans. Ind. Electron.* **66** 5374–82
[17] Wang Y, Xu Z and Huang H 2020 *Smart Mater. Struct.* **29** 125006
[18] Rakotondrabe M, Haddab Y and Lutz P 2008 *IEEE Trans. Control Syst. Technol.* **16** 1316–22
[19] Duan Y, Peng H, Zhu Y, Shen Y and Ling J 2023 Inertial piezoelectric actuation of a needle insertion device for minimally invasive surgery *2023 IEEE Int. Conf. on Robotics and Biomimetics (ROBIO)* pp 1–6
[20] Gao Q, He M, Lu X, Zhang C and Cheng T 2019 *J. Intell. Mater. Syst. Struct.* **30** 2125–34
[21] Li H, Wang J, Xu Z, Qin F, Wang Z and Zhao H 2021 *Rev. Sci. Instrum.* **92** 125001
[22] Xun M, Yu H, Zhang S, Chang Q, Deng J and Liu Y 2023 *Smart Mater. Struct.* **32** 055002
[23] Zhu J, Zhong B, Jin Z, He H, Wang Z and Sun L 2018 *Smart Mater. Struct.* **27** 117004
[24] Cheng T, He M, Li H, Lu X, Zhao H and Gao H 2017 *IEEE Trans. Ind. Electron.* **64** 5545–52
[25] Qiao G, Ning P, Xia X, Yu Y, Lu X and Cheng T 2022 *IEEE Trans. Ind. Electron.* **69** 3948–58
[26] Wang X, Huang H, Fan H, Sun W, Li X and Liu J 2019 *Sens. Actuators* A **295** 348–56
[27] Wang X, Zhu L and Huang H 2021 *IEEE Trans. Ind. Electron.* **68** 11266–75
[28] Li H, Wang J, Xu Z, Qin F, Wang Z, Zhu H and Zhao H 2023 *Mech. Syst. Signal Process.* **186** 109752
[29] Yang Z, Zhou X, Huang H, Dong J, Fan Z and Zhao H 2020 *IEEE Trans. Ind. Electron.* **67** 3870–8
[30] Tian X, Chen W, Zhang B and Liu Y 2022 *IEEE Trans. Ind. Electron.* **69** 10396–406
[31] Tang J, Fan H, Liu J and Huang H 2020 *Mech. Syst. Signal Process.* **143** 106855
[32] Yang X, Tang J, Guo W, Huang H, Fan H, Liu J and Li T 2021 *Actuators* **10** 200
[33] Qiu C, Ling J, Zhang Y, Ming M, Feng Z and Xiao X 2021 *Mech. Mach. Theory* **159** 104254
[34] Liu Y, Xu Z, Li X, Sun W and Huang H 2022 *Mech. Syst. Signal Process.* **172** 108999
[35] Li J, He L, Cai J, Hu Y, Wen J, Ma J and Wan N 2021 *Smart Mater. Struct.* **30** 085030
[36] Huo Z, Tian Y, Wang F, Zhang W, Shi B and Zhang D 2022 *IEEE/ASME Trans. Mechatronics* **27** 3053–64
[37] Li J, Chen S, He L, Jian J, Hu Y, Wen J, Chen S and Kan J 2023 *IEEE/ASME Trans. Mechatronics* **28** 1326–36
[38] Li Y, Yuan L, Wang L, Si X, Xue J, Wang R and Luo G 2024 *Sens. Actuators* A **379** 115948
[39] Dong J, Zhang B, Li X, Xu Z, Wang J, Liu C and Cao Y 2021 *Smart Mater. Struct.* **30** 095015
[40] An Y, Ji S and Zhao J 2023 *IEEE Trans. Ind. Electron.* **70** 9301–11
[41] Li H, Wang J, Xu Z, Qin F, Wang Z and Zhao H 2023 *J. Intell. Mater. Syst. Struct.* **34** 364–76